Behavior and surface properties of microalgae indicate environmental changes

N. Ivošević DeNardis[1*], N. Novosel Vlašić[1], T. Mišić Radić[1], J. Zemła[2], M. Lekka[2], I. Demir-Yilmaz[3,4], C. Formosa Dague[3], M. Levak Zorinc[1], I. Vrana[1], K. Juraić[1], L. Horvat[1], P. Žutinić[5], M. Gligora Udovič[5], B. Gašparović[1]

[1]*Ruđer Bošković Institute, Zagreb, Croatia, [2]Institute of Nuclear Physics Polish Academy of Sciences, Kraków, Poland, [3] TBI, Université de Toulouse, INSA, INRAE, CNRS, Toulouse, France, [4]LAAS, Université de Toulouse, CNRS, Toulouse, France, [5]Department of Biology, Faculty of Science, University of Zagreb, Zagreb, Croatia*

ORCID's

Nadica Ivošević DeNardis, 0000-0002-3635-4869

Nives Novosel Vlašić, 0000-0002-7528-017X

Tea Mišić Radić, 0000-0002-2523-4749

Joanna Zemła, 0000-0003-0980-4649

Malgorzata Lekka, 0000-0003-0844-8662

Irem Demir Yilmaz, 0000-0002-5758-206X

Cecile Formosa Dague, 0000-0002-8627-3784

Maja Levak Zorinc, 0000-0003-4662-1059

Ivna Vrana, 0000-0002-2712-2708

Krunoslav Juraić, 0000-0001-9653-7723

Lucija Horvat 0009-0004-7097-7615

Petar Žutinić, 0000-0002-9836-9636

Marija Gligora Udovič, 0000-0002-1982-2528

Blaženka Gašparović, 0000-0001-5888-2139

Corresponding author:

N. Ivošević DeNardis

Tel: +385 1 4561-128

E-mail address: ivosevic@irb.hr

Abstract

We conducted a microcosm experiment under near-natural conditions to investigate the effects of environmental stressors, temperature and salinity, on the response of three microalgal species. The microalgae responded to increased temperature and altered salinity by adapting at behavioral, mechanical, and molecular levels. The response of microalgae is species-specific, with cell barrier complexity playing an important protective role. With decrease in salinity, the green flagellar cells of *Dunaliella tertiolecta* vibrate around the point and become stiff while their physiological activity is the highest, which may indicate that organic matter is released into the medium. At the highest salinity, *Tetraselmis suecica* demonstrated the highest growth rate along with the hydrophobic behavior of cells, which acts as a favorable condition for aggregate formation. Under these conditions, the cells could enter the cyst stage, while the content of polar lipids could mediate cell adhesion to the natural interfaces. *Cylindrotheca closterium,* a diatom with an organosilicate cell wall, also showed the highest physiological activity at decreasing salinity. However, the cells were softest and exhibited hydrophilic behavior, implying that released organic material could alter the surface properties of diatom. This study provides insight into the behavior and surface properties of microalgae under near-natural conditions, which may contribute to a fundamental understanding of how biochemistry and mechanics interact to control the functional behavior of microalgal cells in climatically altered aquatic systems.

Keywords: cell surface properties, environmental stress, hydrophobicity, microalgae, motility, released organic matter

1. Introduction

Understanding the effects of various environmental stressors on microalgae is critical for assessing the health and function of aquatic habitats, in terms of nutrient cycling and ecosystem stability (Zhang et al. 2022; Khollsi et al. 2023). Multiple stressors such as temperature, salinity, pH, light intensity, nutrient availability, and pollution can significantly affect the growth, productivity, physiology, and overall status of microalgae by acting independently or interacting with each other, leading to complex cellular responses (Borowitzka 2018; Schriber and Venable 2019; Wu et al. 2021; Haris et al. 2022; Farkas et al. 2023). The response of microalgae to various stressors depends on the species, the type, the duration and intensity of the stressors. Some microalgae may exhibit tolerance or acclimatization mechanisms that allow them to withstand certain stress combinations better than others. However, in many cases, prolonged exposure to multiple stressors can lead to significant declines in microalgal populations, disruption of aquatic ecosystems, and possible cascading effects at higher trophic levels (Häder and Gao 2015; Murphy et al. 2020; Van de Waal and Litchman 2020; Glibert et al. 2022). Stressors can impair photosynthesis, disrupt cellular processes, and even lead to cell death. Various stress conditions, e.g., increased temperature combined with nutrient deficiency, can cause a range of cellular physiological, mechanical, and metabolic changes that promote lipid production, which is essential for biofuel production and other applications (Arbona et al. 2013; Kwak et al. 2016; Flanjak et al. 2022). Bautista-Chamizo et al. (2018) reported an increased production of microalgal lipids and carotenoids in *Phaeodactylum tricornutum* cells under synergistic effects of pH, salinity, and temperature. To decipher the complex interplay of abiotic stressors on microalgae in aquatic systems, we mimicked the seasonal variation of individual stressors on three microalgae under laboratory conditions (Novosel et al. 2022a, b). The results showed that the response of microalgae was species-specific and stressor-dependent. With a decrease in temperature or salinity, cells became stiffer and hydrophobic due to increase in sterol content, while the increase in physiological activity of cells presumably decreased cell motility. Due to strong cellular response, the naked green alga *Dunaliella tertiolecta* showed the greatest chemical and nanomechanical changes. *Tetraselmis suecica*, a green alga with calcite-coated theca, appeared to be temperature tolerant but salinity-sensitive. In contrast, the diatom *Cylindrotheca closterium* was less susceptible due to the protective function of its organosilicate cell wall.

Given the ecological importance of microalgae in aquatic ecosystems, it is of greatest research interest to better understand the responses of microalgae to environmental stressors,

3

such as temperature and salinity, which are known abiotic indicators of climate change (Velasco et al. 2019). To date, a few laboratory studies have reported results at the single cell level, focusing specifically on the barrier properties of microalgae and the behavior of microalgae when exposed to a single stressor (Pletikapć et al. 2012; Ivošević DeNardis et al. 2019; Pillet et al. 2019; Novosel et al. 2020, 2022 a, b; Mišić Radić et al. 2021, 2022; Demir-Yilmaz et al. 2023 a, b). The aim of this study was to investigate the effects of increased temperature and altered salinity on the response of microalgae under near-natural conditions. We selected three model species of microalgae in aquatic systems with contrasting structures of the cell barrier. We hypothesized that: (i) all selected microalgae would acclimate to environmental stressors by changing at behavioral, mechanical, and molecular levels, and (ii) microalgae with cell walls would acclimate more readily. The results will provide insights into the underlying mechanisms of microalgal response that are critical to understanding the impacts of climate change on marine ecosystems.

2. Materials and methods

2.1. Microcosm setup

Three different species of marine algae were selected: *Dunaliella tertiolecta* (DT, Chlorophyta, CCMP 1320, Culture Collection Bigelow Laboratory for Ocean Sciences, Bigelow, MN, USA), *Tetraselmis suecica* (TS, Chlorophyta, CCAP 66 / 22A, Collection and Protozoa, Scottish Marine Institute, Oban UK), and *Cylindrotheca closterium* (CC, Bacillariophyta, CCMP 1554, Culture Collection Bigelow Laboratory for Ocean Sciences, Bigelow, MN, USA). Microalgal cells were cultured in 1 L of F/2 growth medium (Guillard 1975) prepared with natural seawater filtered through Whatman filter with a pore size of 0.22 μm and with three selected salinities: 19, 27 and 38. Cell cultures were grown outdoors in 2 L Nalgene PC bottles in a natural light-dark cycle. A total of 18 bottles of cell cultures and 6 bottles of seawater of the appropriate salinities as controls were placed in a swimming pool at a location with maximum possible daily sunlight from September 8 to 14, 2022 (Fig. 1). The swimming pool (MSpa Lite, MSpa UK Ltd., Hitchin, UK) had the following characteristics: volume 960 L, height 70 cm, outer diameter 2.04 m, inner diameter 1.60 m. To ensure good mixing of the samples, a nozzle was placed at the bottom of the pool, which was operated by a water pump in a closed circuit. This nozzle was placed at the edge of the basin at an angle of approximately 45°, creating waves and counterclockwise circulation of the water in the basin. The bottles containing 1 L samples were allowed to float freely at 2 rpm within the basin perimeter, with the observed wave amplitude

4

of 1-5 cm. A digital temperature logger was placed in the swimming pool to record the water temperature every 10 minutes (Fig. 2). The fluctuations in air temperature followed the same pattern as the fluctuations of water temperature in the pool. The water temperature was on average 3°C higher than the air temperature. Cell cultures were grown in the pool at water temperature of 28-33°C. To ensure the culturing of selected microalgal species under selected environmental stressors, a replicate set of experiments (at salinities of 19, 27, 38 and temperature of 30°C) was performed in the laboratory. The cell abundances in the replicate samples were determined each day using a Fuchs-Rosenthal hemocytometer (Fein-Optik Jena, Jena, Germany, depth 0.2 mm) and a light microscope (Olympus BX51, Olympus Corporation, Tokyo, Japan). The growth rate and doubling time of cells were determined in the exponential growth phase from day 3 to day 5 (Kim 2015). In the stationary growth phase (day 7), the cells were centrifuged (2000 x g, 3 min) and the pellets were resuspended twice with seawater. The stock cell suspension was prepared by resuspending the last pellet in 2 mL of filtered seawater with the appropriate salinity.

2.2. Confocal microscopy

Confocal measurements were carried out using an oil immersion objective (63x magnification) and a white-light laser on a Leica TCS SP8 Laser Scanning Confocal Microscope (Leica Microsystems GmbH, Wetzlar, Germany). The spectral scan option was used to enhance the ranges of emission and excitation wavelengths. Autofluorescence of algal cells was detected at a maximum excitation wavelength of 650 nm and a detection wavelength range of 720-750 nm.

2.3. Sample preparation for confocal imaging

Slides for confocal microscopy were washed in glass beakers with ethanol followed by ultrapure water. The slides were dried with a stream of nitrogen. An aliquot of 50 µL of 0.2% (w/v) polyethyleneimine (PEI, Sigma Aldrich Corporation, St. Louis, MS, USA) was added to the center of the clean slide to prepare for cell immobilization and allowed to settle for 30 minutes. After removing the PEI droplet, the center of the slide was rinsed three times with ultrapure water. Then, 20 µL of the cell cultures were added to the center of the slide and allowed to settle. The slides were kept in a Petri dish with moist absorbent paper until imaging to prevent evaporation of the droplets. Prior to imaging, samples were stained with DAPI (Sigma), Alcian blue (Sigma), and DiI (Sigma) by diluting 20x stock solutions.

2.4. Motility analysis

The motility of cells was recorded as 10 consecutive video clips (.avi format, duration 5 s, 50-60 frames per second, image size: 340 x 250, 4x4 binning) under an Olympus BX51 microscope (10x magnification). For analysis of cell motility and trajectories, video data were fed into the open-source image processing software ICY (http:icy.bioimageanalysis.org; Novosel et al. 2020). The Spot Tracking, Track Manager, and Motion Profiler plug-ins were used. ICY produced an ASCII file that contained sample size, spatiotemporal position of the cells, number of motile and non-motile cells, minimum, median, arithmetic mean, and maximum speeds and search radius. The search radius is defined as the farthest distance that a cell can go from its origin. Data from around 300 cell analyses were imported into Microsoft Excel (Microsoft Corporation, Redmond, WA, USA). The software tool RStudio was used for additional statistical analyzes (R 2022 RStudio 2023). Boxplots of cell speed and search radius were generated. The Shapiro-Wilk normality test (Royston 1995) and the Kruskal-Wallis ANOVA test (Bauer 1972; Hollander 1999) were used to examine the distributions and compare the mean values of cell speed and search radius under environmental stressors in near-natural conditions.

2.5. Electrochemical method

Molecular adsorption on the dropping mercury electrode (DME) was used to characterize the organic constituents, such as biopolymers and sub-micrometer particles, in the aqueous electrolyte solution using the electrochemical method of polarography (Žutić et al. 1999, 2004; Svetličić et al. 2006; Pletikapić and Ivošević DeNardis 2017). The adsorption of organic molecules on DME is recorded as a gradual decrease in the reduction current, which is proportional to the surfactant concentration in the sample and is referred to as surfactant activity. Surfactant activity provides an alternative method for determining the amount of dissolved organic carbon in seawater (Hunter and Liss 1981). The polarographic maximum of Hg(II) ions can be used to evaluate surfactant activity, expressed in milligrams per liter as the equivalent amount of the non-ionic synthetic surfactant Triton-X-100 (polyethylene glycol tert-octylphenyl ether).

2.6. Electrochemical measurement of cell sample

Cell samples were characterized electrochemically using a three-electrode system in an air-permeable and thermostatic Metrohm vessel. The working electrode, DME, had the following characteristics: drop time of 2.0 seconds, flow rate of 6.0 mg s^{-1}, and maximum surface area of

4.57 mm^2. All potentials were compared to a potential measured on a reference electrode. This consisted of a ceramic frit separated from the measured dispersion by Ag/AgCl (0.1 M NaCl). The counter electrode consisted of a platinum wire. An aliquot of the cell suspensions was mixed with 25 mL of filtered seawater (pH 8.0) and placed in a Methrom vessel at 20°C. A 174A Polarographic Analyzer (Princeton Applied Research, Oak Ridge, TN, USA) connected to a computer was used for electrochemical measurements. Analogue data were acquired using a DAQ card-AI-16-XE-50 (National Instruments, Austin, TX, USA). The program written in LabView 6.1 software (National Instruments, Austin, TX, USA) was used to analyze the data. Cell samples were electrochemically characterized by recording polarograms of oxygen reduction (current-potential curves). Prior to the measurement of surfactant activity, 0.5 mL of 0.1 M HgCl$_2$ was added to the sample.

2.7. Atomic force microscopy (AFM)

A Multimode Scanning Probe Microscope with a Nanoscope IIIa controller (Bruker, Billerica, MA, USA) and a vertical engagement (JV) 125 m scanner was used for imaging cells and released extracellular poylmers. A DNP probe (Bruker, Billerica, MA, USA) with a nominal spring constant of 0.06 N m^{-1} and a nominal frequency of 18 kHz was employed for contact mode imaging in the air. The scan resolution was 512 samples per line and the linear scan rate was optimized between 1.5 and 2 Hz. To reduce the forces between the tip and the surface, the set point was kept as low as possible. Image analysis was performed using NanoScopeTM software (NanoScope Analysis, version 2.0; Bruker, Billerica, MA, USA).

2.8. Sample preparation for AFM imaging of cells and released extracellular polymers

Samples for AFM imaging of cells and released extracellular polymers were prepared according to a previously established protocol (Novosel et al. 2022 a, b). Briefly, DT, TS, and CC cells were separated from the growth medium by centrifugation (section 2.1). The collected pellets were then used to prepare the samples for AFM. Unmodified mica was used as substrate for the preparation of DT and CC samples, while mica modified with PEI was used for the preparation of the TS sample. The sample preparation protocol for AFM imaging only required fixation of the DT suspension. Prior to AFM imaging, samples were rinsed three times with ultrapure water to remove excess salt crystals and dried in closed Petri dishes for 45 minutes.

2.9. Atomic force microscopy working in force spectroscopy mode

Mechanical properties of algal cells were measured using an AFM JPK NanoWizard 4 XP (Bruker, Berlin, Germany) operating in force spectroscopy mode. The microscope is integrated with an inverted optical microscope (Olympus IX73, Olympus Corporation, Tokyo, Japan) using LUCPLFLN40XPH objective (Olympus Corporation, Tokyo, Japan), which allows direct superposition of the optical image of the sample and the scan area. A silicon nitride pyramid probe, MLCT-D (Bruker, Billerica, MA, USA) with a nominal spring constant of 0.03 N m^{-1}, a nominal frequency of 15 kHz, and the half-open angle of the probe of 21° was used. The cantilevers spring constants were calibrated using the thermal noise method (Sader et al. 1995). Force curves were recorded over a 3 µm × 3 µm area in the central part of the cell at an approach and retraction velocity of 8 µm s^{-1} and a loading force of 2 nN. A grid of 4×4 force curves was recorded. The number of cells measured varied from 20 to 35 cells.

The mechanical properties of the CC cells were measured using the Nanowizard III AFM system (Bruker, Berlin, Germany). Force spectroscopy experiments were performed with an applied force between 1 and 2 nN using MLCT AUWH cantilevers with nominal spring constants of 0.01 N m^{-1}. Nanoindentation measurements were performed on 7 cells, and 400 force curves were recorded on areas of 1 µm × 1 µm on the cell surface.

Measurements for all three species were performed at salinities of 19, 27, and 38. JPK data processing software (Bruker-JPK, Berlin, Germany), version 7.0.165 was used for data analysis.

2.10. Elasticity determination

The apparent Young's modulus (elasticity parameter, *E*) for DT and TS was determined by applying the Hertz-Sneddon contact model (Sneddon 1965), which relates the loading force (*F*) and the indentation depth (*δ*) in the case of a four-sided pyramid probe as follows:

$$F = \frac{E}{1-\nu^2}\frac{tan\alpha}{\sqrt{2}}\delta^2 \tag{1}$$

In the equation above, α is a half-open angle of the indenting probe and ν is Poisson's ratio equal to 0.5 because we assume incompressibility of the algal cells. The maximum indentation depth did not exceed 2 µm, and the model was fitted to the AFM data over the entire range of indentation depths. The value *E* of CC were calculated from 50 nm indentation curves using the

Hertz-Sneddon model (Hertz, 1881) for a conical indenter in which the force F, indentation depth (δ), and E follow equation (2):

$$F = \frac{2E \tan\alpha}{\pi (1 - \nu^2)} \delta^2 \qquad (2)$$

Here α is the opening angle of the tip (17.5°) and ν is the Poisson's ratio (which is arbitrarily assumed to be 0.5). The spring constants of the cantilevers were determined before each experiment using the thermal noise method (Hutter and Bechhoefer 1993).

The calculated E are quantified as the median and the first (Q1) and third (Q3) quartiles. Statistical comparisons of the results obtained in each case were performed using an unpaired t-test, which allowed us to compare the means of two independent groups (p < 0.001).

2.11. Hydrophobic properties of cells

The hydrophobic properties of DT and TS were quantified by comparing AFM data obtained with unmodified and trichloroctadecylsilane (OTS; Sigma-Aldrich Corporation, St. Louis, MS, USA) functionalized MLCT-D probes. The vapor deposition of the OTS silane containing hydrophobic $-CH_3$ functional groups was performed in a vacuum (2 h exposure). The adhesion properties of cells were quantified by the work of adhesion (W_{adh}) parameter, which was determined from the negative part of the retraction force curve. The forces acting between the algal cell and the probe (unmodified and $-CH_3$ modified) for the duration of the experiment cause deflection of the cantilever. The functionalization of the probe was performed immediately before the measurements. The probe speed, scan range, map density, and number of cells examined were the same as those used in the mechanical studies (Section 2.9). The degree of algal cell hydrophobicity (ΔW_{adh}) was determined using the following equation:

$$\Delta W_{adh} = W_{adh(noOTS)} - W_{adh(OTS)} \qquad (3)$$

where $W_{adh(noOTS)}$ and $W_{adh(OTS)}$ are the work of adhesion extracted from force curves collected with bare and CH_3-functionalised AFM cantilevers, respectively.

In the case of CC, hydrophobic properties were studied using a recently developed method consisting of measuring the interactions between a bubble (hydrophobic surface) and cell surfaces using fluidic force microscopy (FluidFM; Demir et al. 2021). For this purpose, FluidFM probes with an aperture of 8 µm in diameter (Cytosurge AG, Opfikon, Switzerland)

were hydrophobized by coating with self-assembled monolayers (SAMs) of silanes using SAMs vapor deposition technique. The FluidFM cantilevers were functionalized with 1H,1H,2H,2H-perfluorodecyltrichlorosilane (FDTS) using an Orbis-1000 equipment (Memsstar, Livingston, UK) to make their outer and inner surfaces of the microchannel hydrophobic. The deposition was carried out under vacuum at 40 Torr and -40°C for 5 minutes. Then, the microchannel of these silanized cantilevers was filled with air and the probe was immersed in PBS 1X. A slight overpressure of 20 mbar was applied to remove any particulate or dust contamination or to prevent clogging of the FluidFM cantilever. To create a bubble at the opening of the cantilever, a positive pressure of 200 mbar was then applied inside the microfluidic cantilever in buffer. The silanized probes were calibrated using the thermal noise method before each measurement (Hutter and Bechhoefer 1993). The interactions between the generated bubbles and CC cells under different conditions were then recorded in force spectroscopy mode, applying a maximum force of 1 nN and a constant retraction speed of 2 µm s^{-1}. For each condition, areas of 0.5 µm × 0.5 µm were examined on 5 different cells. Adhesion forces were determined by calculating the maximum adhesion force from the obtained retraction force curves.

2.12. Sample preparation for force spectroscopy measurements

PEI-coated microscopic glass slides (Heinz Herenz Medizinalbedarf GmbH, Hamburg, Germany) were used as substrates for the immobilization of algal cells. A volume of 200 µL of a 0.1% PEI solution was added to a clean (ethanol and dH$_2$O sonication for 15 min each) glass slide and dried overnight.

Cell suspensions were prepared according to protocols optimized for each of the cell types studied. In the case of CC, a 200 µL cell suspension was placed on a substrate for 1 h. The sample was then rinsed 3 times with 200 µL of filtered seawater. The following procedure was used to isolate cells of DT and TS. An aliquot of 1.5 mL of DT and TS suspensions were taken from the corresponding culture bottles and transferred to Eppendorf tubes. The suspensions were then centrifuged at 265 × g for 3 min and at 940 × g for 5 min (DT and TS, respectively). Then, 1 mL of the medium was removed and the pellet was vortexed. An additional volume of seawater (1 mL) was added to the cell suspensions and centrifuged at the same speed and duration. The supernatant was removed and the cells were resuspended in 400 µL of the filtered seawater. Next, 100 µL of cell suspension was added on a PEI-coated glass slide. After 30 min, the samples were rinsed 3 times with 100 µL of filtered seawater and measured with AFM.

2.13. Lipid extraction

For the determination of lipid classes, we collected 100-200 mL of cell culture suspension, which was filtered through 0.7 µm Whatman GF/F filters and pre-combusted at 450°C for 5 h. Lipids were extracted according to a slightly modified protocol of Bligh and Dyer (1959): 10 mL dichloromethane/methanol/deionized water (1:2:0.8 v/v/v) was added to the sliced filters in the cuvettes, along with methyl stearate, which was added as an internal standard to calculate lipid recovery. After 3 min of sonication, the filters were stored in dichloromethane/methanol/deionised water overnight at 4°C. Afterwards, the mixture of filter and monophasic solution was filtered through a sinter funnel into a separatory funnel, washed with 10 mL of monophasic solution, and washed with 10 mL of the dichloromethane/0.73% NaCl (1:1 v/v) solution mixture. The lipids dissolved in dichloromethane were collected and the extraction was performed again with 10 mL of the dichloromethane. The extracts were evaporated to dryness under nitrogen gas and redissolved in 50 µL of dichloromethane before analysis.

2.14. Lipid analysis

Lipid classes were analyzed by thin-layer chromatography/flame ionization detection (TLC/FID; Iatroscan MK-VI, Mitsubishi Kagaku Iatron, INC, Tokyo, Japan). Separation of lipid classes was performed using Chromarods SV and quantified by external calibration with a standard lipid mixture. Hydrogen flow was set at 160 mL min^{-1} and air flow at 2000 mL min^{-1}. The standard deviation determined from duplicate runs ranges from 0.00-0.42 pg cell^{-1} and depends on the lipid class and microalgae. This technique detects 18 lipid classes (hydrocarbons, steryl esters (SE), fatty acid methyl esters, ketones, triacylglycerols, free fatty acids, alcohols, 1,3-and 1,2-diacylglycerols, sterols, pigments, monoacylglycerols, three glycolipids (monogalactosyldiacylglycerols, digalactosyldiacylglycerols, sulfoquinovosyldiacylglycerols), three phospholipids (mono- and di-phosphatidylglycerols, phosphatidylethanolamines and phosphatidylcholines). The separation involved subsequent elution in solvent systems of increasing polarity followed by partial combustion of the Chromarods (Gašparović et al. 2015, 2017). For this work we considered cell lipids as nonpolar polar, and also membrane lipids.

3. Results

3.1. Microalgal growth dynamics

We conducted a microcosm experiment involving three microalgal species (DT, TS, CC) grown at three selected salinities and elevated temperature to mimic environmental stressors under near-natural conditions. Fig. 3 shows the growth curves of DT, TS and CC at salinities of 19, 27, and 38, respectively, and pool water temperatures of 28 to 33°C. The initial number of inoculated cells in the growth media was approximately 5.0×10^4 cells mL^{-1} for all species studied. On day 7, all cells mostly entered stationary phase and samples were collected for further characterization. Table S1 summarizes the growth rate and doubling time for each cell species under the selected conditions. The fastest growth and thus the shortest doubling time were obtained for DT and CC at a salinity of 27, and for TS at a salinity of 38.

Fig. S1 shows representative overlaid confocal images of DT, TS, CC cell cultures under environmental stressors in near-natural conditions. Confocal images of DT cultures at salinities of 38 and 27 showed single cells, presence of single bacterial material, and a strong autofluorescence signal, while at salinity 27 some aggregates were found. In contrast, at salinity of 19, major morphological changes occurred in the DT cells including granular surface structure, detached flagella, some cell aggregates, and presence of bacterial material. In the TS cell culture, cells appeared without flagella at all salinities; at salinity of 19, the autofluorescence signal was weak, cells formed no aggregates, and no bacteria were detected. Confocal imaging of CC cultures at salinities of 38 and 27 showed a few aggregates, very few individual bacteria, and some amorphous particles. At salinity of 19, the cell rostra became curved, and some bacteria and amorphous microaggregates were visible. No bacterial aggregates were observed with DAPI staining.

3.2. Motility of flagellated species

Fig. S2 shows the reconstructed trajectories of individual DT cells under environmental stressors under near-natural conditions. At salinity of 19, 43% of the cells were nearly immobile or vibrated at the spot. At salinity of 27, 19% of the cells were static, while the rest moved. At salinity of 38, the majority of cells (72%) showed significant motility. At salinities of 19, 27, and 38, the average speed of vibrating and motile cells were 14, 27, and 30 μm s^{-1} and 68, 57, and 76 μm s^{-1}, respectively (Tables S2.1).

Fig. 4a shows boxplots of cell speeds for the entire DT population. The median speed at salinities of 19, 27, and 38 were 44, 47, and 59 μm s^{-1}, respectively (Table S2.2a). Fig. 4c shows boxplots of the search radii of DT cells. For salinities of 19, 27, and 38, the median search radii were 4 μm, 19 μm, and 7 μm, respectively (Table S2.2b). At salinities of 19, 27, and 38, the set of cells that moved regularly had an average search radius of 35 μm, 36 μm, and 39 μm, respectively. According to results of the Shapiro-Wilk normality test, the data for search radius and average speed does not follow normal distribution (Table S3.3), except for the results on DT for salinities of 19 and 38. There was a weak indication that lower salinity decreased average speed for both DT and TS, but the results of the Kruskal-Wallis ANOVA test showed that this variation in average speed and search radius were not statistically significant (Table S3.4).

Fig. S3 shows the reconstructed trajectories of individual TS cells under environmental stressors in near-natural conditions. At salinities of 19, 27, and 38, between 23% to 33% of the cells were stationary with an average speed from 32 to 47 μm s^{-1}, while the majority of cells showed pronounced movement with an average speed in the range between 93 to 114 μm s^{-1}, depending on salinity gradient (Table S3.1.).

Fig. 4b shows the boxplots of the cell speeds for the entire TS population. The median cell speed was 61 μm s^{-1}, 79 μm s^{-1}, and 67 m s^{-1} for salinities of 19, 27, and 38 (control), respectively, with no statistically significant deviation from the control (Table S3.2a). The average speed of a set of uniformly moving cells grown at 19, 27, and 38 was 99 μm s^{-1}, 114 μm s^{-1}, and 93 μm s^{-1}, respectively (Table S3.1). Boxplots of the TS cells with search radius are shown in Fig. 4d. The median search radius at salinities of 19, 27, and 38 were 4 μm, 5 μm, and 5 μm, respectively. The group of substantially moving cells grown at salinities of 19, 27, and 38 had an average search radius of 22 μm, 33 μm, and 54 μm, respectively (Table S3.2b).

3.3. Electrochemical characterization of released surface-active organic matter

The cell releasing surface-active organic matter can be determined by measuring the current-potential curves of Hg(II), which is proportional to surfactant activity. The sample's surfactant activity is a quantitative assessment of the physiological activity of the cells exposed to environmental stressors in near-natural conditions. The results showed that the surfactant activity of the cells steadily increased as the salinity decreased to 19 (Fig. 5). At salinity of 19, all cells studied had the highest surfactant activity, with the TS cell culture having the highest surfactant activity.

3.4. Nanoscale imaging of algal cell and released extracellular polymers

The morphology of algal cells exposed to environmental stressors in near-natural conditions was characterized by AFM. All three species maintained the same basic shape regardless of the selected conditions (Figs. 6a,c,e). The cells of DT had an ovoid shape and contained two flexible flagella. At all salinities studied, the cells of TS had an ellipsoidal shape, and the cell surface had granular features, while all four flagella were absent. The cells of CC had an elongated shape with flexible rostrae that were distinct from the centre of the cell. The raphe, valve, and girdle band, three morphologically distinct elements, were all visible on the cell. The morphological parameters of the cells (length, width, height, and surface roughness) that had grown under environmental stressors are shown in Table S4. The length of the cells of DT grown at salinities of 27 and 38 was similar and lower than that of the cells grown at salinity of 19, while the height at salinity of 19 showed the lowest value. The length and height of the cells of TS increased with increasing salinity, while the width of the cells was similar at all three salinities. The length and width of the cells of CC were similar at all salinities, while the height showed the highest value at a salinity of 19.

The supramolecular organization of the released extracellular polymers (EPS) of the cells of DT, TS and CC exposed to environmental stressors was characterized by AFM (Figs. 6b,d,f). The material surrounding the cells of DT was largely in the form of single and aggregated globules, with just a few fibrils and no fibrillar network found at all salinities. A fibrillar network was observed around the cells of TS grown at salinity of 38, while spherical material, fibrils, and network fragments were observed at salinities of 19 and 27. Around the cells of CC grown at all salinities, there was mainly spherical material, with some fibrils appearing at salinity of 38.

3.5. Nanomechanical characterisation of algal cells by AFM

Algal cells exposed to environmental stressors under near-natural conditions showed a change in mechanical properties (Fig. 7). At salinity of 38, the elasticity parameter E, which quantifies the mechanical properties of DT, was 1.1 (2.4) kPa. As salinity decreased (27 and 19), the cells became stiffer and E increased to 2.4 (3.8) kPa and 3.9 (3.9) kPa, respectively. TS was also stiffer under unfavorable salinity conditions. With increasing salinity, the values of E decreased from 30 (51) kPa and 30 (55) kPa at salinities of 19 and 27, respectively, to 24 (37) kPa at

salinity of 38. In contrast, CC was less deformable at salinity of 38 (E = 819 (1035) kPa) and the E decreased 2.5-fold at lower salinity.

3.6. Hydrophobic properties of algal cells

The influence of environmental stressors on the hydrophobic properties of DT, TS, and CC under near-natural conditions was determined by AFM force spectroscopy studies. The results showed that regardless of salinity, the outer parts of CC were hydrophilic (Table 1). A similar qualitative trend was observed for DT cells. Only TS showed a transition from a near-neutral (unfavorable growth conditions) to a hydrophobic state (salinity of 38).

In addition, the degree of hydrophobicity was quantified with ΔW_{adh} (Fig. S4). The highest ΔW_{adh} value for DT (0.409 ± 0.038 fJ) was obtained at the lowest salinity. As salinity increased, the dominance of hydrophilic properties decreased, ΔW_{adh} of 0.222 ±0.031 fJ. An opposite behavior was observed for TS, characterized by strongly hydrophobic properties at salinity of 38 (ΔW_{adh} = -0.57 ± 0.11 fJ).

3.7. Lipid characterization of algal cells

The change in the amount of polar and nonpolar lipids per cell under selected environmental stressors for the three microalgal species studied is shown in Fig. 8. The change in the proportion of polar lipids relative to total cell lipids is also indicated. The content of cell lipids was the highest in TS, but it was salinity-dependent. The lowest content was observed at the more favorable condition of salinity of 38. At salinities of 27 and 19, the cell lipid content increased along with the increase in the relative content of polar lipids compared to salinity of 38. In contrast to the other two microalgae, CC had a higher relative content of polar lipids than nonpolar lipids, with the content of polar lipids increasing with decreasing salinity from 38 to 19. The cell lipid content of DT was the lowest among the three microalgae studied. The relative content of polar lipids decreased from salinity of 38 to salinity of 19 in both green microalgae studied, DT and TS. The content of membrane lipids of the studied DT, TS and CC followed that of cell lipids (Fig. 9). The data showed that the content of sterols, glycolipids and phospholipids increased with decreasing salinity in all microalgal species.

4. Discussion

We conducted a microcosm experiment as a small-scale model of a specific environment to investigate the response of three microalgal species exposed to environmental stressors under near-natural conditions and to test the relevance of our previously reported laboratory studies with single stressors (Novosel et al. 2022 a, b). We examined the effects of environmental stressors (variation in salinity with elevated temperature) under near-natural conditions on cell growth dynamics, nanomorphology, motility, physiological activity, nanomechanical properties, biochemical changes related to hydrophobicity, and lipid profile. The results showed that all three microalgal species successfully acclimated to environmental stressors under near-natural conditions. As expected, the growth rate of all species was faster under near-natural conditions than under laboratory conditions (Table S1, Novosel et al. 2022b).

Under environmental stressors in near-natural conditions DT showed no change in cell speed, whereas the cells vibrated on the spot (Fig. 4a, c). Interestingly, the mean cell speed of DT under environmental stressors was close to that under single stressor of salinity, indicating the thermotolerant nature of the cells (Ben-Amotz and Avron 1990; Jahnke and White 2003; Pick and Avidan 2017). When salinity was lowered to 19, responses such as decreased growth rate, highest physiological activity, and increase in cell stiffness occurred, most likely due to increased concentration of sterols that contribute to decrease in membrane fluidity (Table S1, Figs. 5, 7, 9). These results are consistent with previous studies (Sheffer et al. 1986; Zelazny et al. 1995; Francavilla et al. 2010; Vrana et al. 2022). *Dunaliella* cells mainly maintained their hydrophilicity under environmental stressors (Figs. 8, S4), which was consistent with the predominant ratio of polar lipids (Fig. 9, Vrana et al. 2022).

In contrast to the laboratory study with DT cells using a single stressor (i.e., salinity of 19 and a temperature of 18°C were considered as control conditions), the stiffness of cells also increased, while DT showed hydrophobic behavior, as was also observed in an additional set of laboratory experiments and double stressors (salinity of 19 and a temperature of 30°C, data not shown here). Thus, the response of microalgae appeared to be more pronounced when cells were stressed with salinity than with temperature under laboratory conditions (Novosel et al. 2022b). On the other hand, a complex interplay of environmental stressors under near-natural conditions leads to a species-specific response without obvious dominance of the stressor.

The mean cell speed of TS was about 3 times lower under near-natural conditions, than under the same salinity and 18°C in laboratory conditions. When salinity was lowered to 19 in near-natural conditions, physiological activity was the highest, cell stiffness increased, and the

16

same nanomechanical behavior was seen as in cells exposed to a single salinity stress (Figs. 5 and 7). *Tetraselmis* cells behaved in a balanced manner at salinities of 19 and 27 and elevated temperature (Table 1). A striking change occurred at salinity of 38, at which the recorded cell growth rate was the highest (Table S1). TS showed hydrophobic behavior (Fig S4), while the predominant content of polar lipids (Fig. 8) could also play an important role in sinking and cell adhesion to natural interfaces (Monteiro et al. 2022). Low hydrophobicity of TS cells was also observed when they were exposed to a single stressor under laboratory conditions (salinity of 38, temperature of 18°C, Novosel et al. 2022b) and at salinity of 38 and a temperature of 30°C (data not shown here). The results also showed that cell stiffness decreased significantly under near-natural conditions in all species studied, in contrast to laboratory conditions, likely due to a complex interplay of environmental stressors under near-natural conditions.

The organosilicate covered diatom CC showed different behavior than the flagellated microalgae, i.e., with salinity decrease CC cells became softer, which could be related to the released organic matter modifying the cell surface (Figs. 5 and 7). In contrast, at salinity of 38, the cells were more stiff even though having the lowest physiological activity. The cells of *Cylindrotheca* showed hydrophilic behavior under the selected environmental conditions, while the ratio of polar lipids was 38-48% (Table 1, Fig. 8). This difference could be due to the fact that hydrophobicity was determined by analyzing 5 single cells and a surface area of 0.5 μm × 0.5 μm, whereas the lipid content was determined from the whole cell culture and was based on disintegrated cell material.

Regarding the nanomorphology of the cells, the results show that the size of DT cells (length and width) was largest at a salinity of 19 under near-natural conditions (Table S4), whereas the cells were largest at a salinity of 38 under single stressor of salinity in laboratory conditions (Novosel et al. 2022b). The cell size of TS was largest at salinity of 38, both in microcosm and laboratory experiments. The cell size of CC was constant in the microcosm experiment, whereas in the laboratory experiment the largest cell size was recorded at salinity of 38.

Regarding the nanostructural organization of the released organic matter, the predominance of globules and the absence of a fibrillar network structure were observed in the EPS of DT under near-natural conditions, as well as when the cells were exposed to salinity change under laboratory conditions (Novosel et al. 2022b). EPS of TS grown under near-natural conditions at salinities of 9, 19, and 27 exhibited fibrillar network structures, whereas cells grown at salinity of 38 did not. The fibrillar network structure in the EPS of TS was also

observed when the cells were subjected to salinity change in the laboratory (Novosel et al. 2022b). The extracellular polymers of CC were mostly present in globular form, whereas the fibrillar material was mostly present when the cells were exposed to a change in salinity under laboratory conditions (Novosel et al. 2022b).

At the molecular level, unfavorable growth conditions often lead to the accumulation of nonpolar lipids, mainly tryacilglycerols (Thompson 1996; Du and Benning 2016; Novak et al. 2019). Tryacilglycerols are stored in droplets in which they are surrounded by a phospholipid monolayer and proteins (Masclaux-Daubresse et al. 2020). The tryacilglycerol droplets are reused for the synthesis of polar lipids when conditions change (Thompson 1996). A study of the effects of temperature on the tryacilglycerols and tryacilglycerol fatty acid composition of the microalga *Dunaliella viridis* revealed that increased temperature resulted in an accumulation of tryacilglycerols, while the fatty acid composition of tryacilglycerols was redistributed toward an increased proportion of the saturated fatty acids (C16:0, C18:0, C20:0, C22:0, C24:0, and C26:0, Srirangan et al. 2015). Both cell content and the proportion of nonpolar lipids increased when two stressors (unfavorable temperature at ~30°C and hypoosmotic shock at salinities of 27 and 19) were combined in green algae DT and TS (Fig. 9). Since cell stiffness was also increased in these two microalgae (Fig. 7), we can assume that DT and TS produce tryacilglycerol droplets that contribute to cell hardness. This was mainly because saturated fatty acids are more compactly bound than unsaturated ones (Niemelä et al. 2006), thus providing to cell hardness. CC had the highest content of nonpolar lipids, indicating this alga to be the most sensitive to stress of the three microalgae studied in near-natural conditions (Fig. 8). Temperature stress significantly increases the strerol content in the membranes of all three algae studied (Fig. 9) compared to cultivation at 18°C (Novosel et al. 2022b). However, while low salinity stress had no effect on the sterol content of DT cells (Novosel et al. 2022b), the sinergy of temperature and hypoosmotic stress increased the ST content. The same trend was also observed in TS and CC. A similar pattern of increase in sterol content induced by an increase in water temperature in batch cultures of three dinoflagellates was also reported by Chen et al. (2019). The observed sterol increase was consistent with the fact that stability, fluidity, and permeability of the lipid bilayer depend on sterols (Benveniste 2004). Zelazny et al. (1995) also confirmed the role of plasma sterols in osmoregulation of two *Dunaliella* species. When *Dunaliella* cells were exposed to hyperosmotic shock, physiological activity increased in terms of inducing glycerol synthesis and synthesis of plasma membrane sterols (Zelazny et al. 1995). The exposure of *Tetraselmis striata* cells to varius abiotic stresses such as nutrient deficiency,

high light intensity, high salinity, and extreme temperatures, resulted in a decrease in biomass productivity, while lipid production was stimulated (Monteiro et al. 2022).

Glycolipid content of DT (Fig. 9) did not differ significantly under the influence of a single stressor (salinity, at 18°C, Novosel et al. 2022b) or environmental stressors under near-natural conditions (~30°C and for three salinities studied). The combination of stressors, high temperature and hyposalinity, resulted in a significant increase in phospholipid content in DT cells (Fig. 9). Similar to DT, the content of phospholipids in TS and CC increased significantly at higher temperatures and when two stressors were combined (Fig. 9). The increase in phospholipid content could be the result of an increased saturated fatty acid content in phospholipids, as was previously observed in diatom *Chaetoceros pseudocurvisetus* (Vrana et al. 2023), in which it facilitated in reducing the membrane fluidization at high temperatures. On the other hand, densely packed saturated fatty acids in the membranes indicate more phospholipids per unit membrane area (Gašparović et al. 2023, submitted), which in turn increases the content of phospholipids in cells. This suggests a greater role of phospholipids in thermal adaptation and adaptation in general. The presumed increase in phospholipid fatty acid saturation was reflected in the increased stiffness of DT at lower salinity and at temperature of 30°C (Fig. 8). While hyposalinity stress alone leads to a decrease in glycolipid content in the cells of TS and CC grown at 18°C (Novosel et al. 2022b), the influence of environmental stressors leads to a substantial increase in the cellular content of glycolipids (Fig. 9), which are found in the photosynthetic apparatus (Siegenthaler 1998).

As far as we know, the effects of environmental stressors on the response of microalgae at the single cell level under near-natural conditions have not yet been integrated in this way. Understanding the surface properties of the cell can facilitate understanding of how biochemistry and mechanics interact to control the functional behavior of cells. Our research has shown that stressed cells exposed to specific temperature, salinity, and salinity-temperature fluctuations exhibited the highest growth rates associated with a change in cell barrier composition and properties, i.e., highest stiffness and hydrophobicity, which could favor cell aggregation (Novosel et al. 2022 a, b; Demir-Yilmaz et al. 2023).

We conclude that the complex interplay of environmental stressors under near-natural conditions leads to a species-specific response of microalgae, with no apparent dominance of stressors. The three selected microalgae with different cell barrier complexity responded to environmental stressors, such as increased temperature and altered salinity, in near-natural environments with changes at behavioral, mechanical, and molecular levels. Under unfavorable

conditions (salinity of 19), all microalgal species exhibited low growth rate but maintained the highest physiological activity. The flagellated species, DT and TS, vibrated around the point and became stiffer, probably due to a higher content of sterols, while the hydrophilicity of the cells could be related to the high content of polar lipids. At the highest salinity, the growth rate of TS is highest and this species showed the most striking changes (e.g., loss of flagella) and exhibited the most pronounced hydrophobicity, which could favor the formation of aggregates, while the concentration of polar lipids could support cell adhesion to natural interfaces. Consequently, the response of TS could indicate progression to the cyst stage. In contrast, the hard, shell-covered diatom CC softened with decreasing salinity, accompanied by maximum physiological activity, which could lead to organic modification of the diatom surface. These results shed new light on the fundamental mechanisms by which microalgae respond to environmental pressures, which are crucial not only for their fate and role, but also for understanding the ecological consequences of climate change on marine ecosystems.

Data availability

The datasets generated during the current study are available from the corresponding author.

References

Bautista-Chamizo E, Sendra M, Cid Á, Seoane M, Romano de Orte M, Riba I (2018) Will temperature and salinity changes exacerbate the effects of seawater acidification on the marine microalga *Phaeodactylum tricornutum*? Sci Total Environ 634:87-94. https://doi.org/10.1016/j.scitotenv.2018.03.314

Bauer DF (1972) Constructing confidence sets using rank statistics. J Am Stat Assoc 67:687-690. https://doi.org/10.2307/2284469

Ben-Amotz A, Avron M (1990) The biotechnology of cultivating the halotolerant alga *Dunaliella*. Trends in Biotechnology 8:121-126. https://doi.org/10.1016/0167-7799(90)90152-N

Benveniste P (2004) Biosynthesis and accumulation of sterols. Annu Rev Plant Biol 55:429-57. https://doi.org/10.1146/annurev.arplant.55.031903.141616

Bligh EG, Dyer WJ (1959) A rapid method of total lipid extraction and purification. Can J Biochem Physiol 37:911-917. https://doi.org/10.1139/o59-099

Borowitzka MA (2018) The 'stress' concept in microalgal biology—homeostasis, acclimation and adaptation. J Appl Phycol 30:2815–2825. https://doi.org/10.1007/s10811-018-1399-0

Chen M, Bi R, Chen X, Ding Y, Zhang H, Li L, Zhao M (2019) Stoichiometric and sterol responses of dinoflagellates to changes in temperature, nutrient supply and growth phase. Algal Res 42:101609. https://doi.org/10.1016/j.algal.2019.101609

Demir, I, Lüchtefeld, I, Lemen, C, Dague, E, Guiraud, P, Zambelli, T, Formosa Dague, C, (2021) Probing the interactions between air bubbles and (bio)interfaces at the nanoscale using FluidFM technology. J Colloid Interface Sci 604: 785–797. https://doi.org/10.1016/j.jcis.2021.07.036

Demir-Yilmaz I, Novosel N, Levak Zorinc M, Mišić Radić T, Ftouhi MS, Guiraud P, Ivošević DeNardis N, Formosa-Dague C (2023a) Investigation of the role of cell hydrophobicity and EPS production in the aggregation of the marine diatom *Cylindrotheca closterium* under hypo-saline conditions. Mar Environ Res 188:106020. https://doi: 10.1016/j.marenvres.2023.106020

Demir-Yilmaz I, Schiavone M, Esvan J, Guiraud P, Formosa-Dague C (2023b) Combining AFM, XPS and chemical hydrolysis to understand the complexity and dynamics of *C. vulgaris* cell wall composition and architecture. Algal Res 72:103102. https://doi.org/10.1016/j.algal.2023.103102

Du ZY, Benning C (2016) Triacylglycerol Accumulation in Photosynthetic Cells in Plants and Algae. In: Nakamura Y, Li-Beisson Y (eds) Lipids in Plant and Algae Development. Subcell Biochem 86. Springer, Cham. https://doi.org/10.1007/978-3-319-25979-6_8

Farkas A, Pap B, Zsíros O, Patai R, Shetty P, Garab G, Bíró T, Ördög V, Maróti G (2023) Salinity stress provokes diverse physiological responses of eukaryotic unicellular microalgae. Algal Res 73:103155. https://doi.org/10.1016/j.algal.2023.103155

Flanjak L, Vrana I, Cvitešić Kušan A, Godrijan Novak T, Penezić A, Gašparović B (2022) The effects of high temperatures and nitrogen availability on the growth and composition of the marine diatom *Chaetoceros pseudocurvisetus*. J Exp Bot 73: 4250-4265. https://doi.org/10.1093/jxb/erac145

Gašparović B, Kazazić SP, Cvitešić A, Penezić A, Frka S (2015) Improved separation and analysis of glycolipids by Iatroscan thin-layer chromatography–flame ionization detection. J Chromatogr A 1409: 259-267. https://doi.org/10.1016/j.chroma.2015.07.047

Gašparović B, Kazazić SP, Cvitešić A, Penezić A, Frka S (2017) Corrigendum to "Improved separation and analysis of glycolipids by Iatroscan thin-layer chromatography–flame ionization detection" [J Chromatogr A 1409 (2015) 259–267]. J Chromatogr A 1521: 168-169. https://doi.org/10.1016/j.chroma.2017.09.038

Glibert PM, Cai W-J, Hall ER, Li M, Main KL, Rose KA, Testa JM, Vidyarathna NK (2022) Stressing over the Complexities of Multiple Stressors in Marine and Estuarine Systems. Ocean-Land-Atmosphere Res 2022: 9787258. https://doi.org/10.34133/2022/9787258

Guillard RRL (1975) Culture of phytoplankton for feeding marine invertebrates. In: Smith WL, Chanley MH (eds) Culture of Marine Invertebrate Animals: Proceedings—1st Conference on Culture of Marine Invertebrate Animals Greenport. Springer US, Boston, pp 29-60.

Häder D-P, Gao K (2015) Interactions of anthropogenic stress factors on marine phytoplankton. Front Environ Sci 3:14. https://doi.org/10.3389/fenvs.2015.00014

Hertz H (1881) Ueber die beruhrung fester elastischer korper. Journal fur die reine und angewandte mathematik 156–171.

Hollander M, Wolfe DA (1999) Nonparametric Statistical Methods. New York: John Wiley & Sons. Pages 27–33 (one-sample), 68–75 (two-sample).

Hunter KA, Liss PS (1981) Polarographic measurement of surface-active material in natural waters. Water Res 15:203-215. https://doi:10.1016/0043-1354(81)90113-5

Hutter JL, Bechhoefer J (1993) Calibration of atomic-force microscope tips. Rev Sci Instrum 64: 1868–1873. https://doi.org/10.1063/1.1143970

Ivošević DeNardis N, Pečar Ilić J, Ružić I, Novosel N, Mišić Radić T, Weber A, Kasum D, Pavlinska P, Katalin Balogh R, Hajdu B, Marček Chorvátová A, Gyurcsik B (2019) Algal cell response to laboratory-induced cadmium stress: a multimethod approach. Eur Biophys J 48:231-248. https://doi.org/10.1007/s00249-019-01347-6

Jahnke LS, White AL (2003) Long-term hyposaline and hypersaline stresses produce distinct antioxidant responses in the marine alga Dunaliella tertiolecta. Journal of Plant Physiology 160:1193–1202. https://doi.org/10.1078/0176-1617-01068

Kholssi R, Lougraimzi H, Moreno-Garrido I (2023) Effects of global environmental change on microalgal photosynthesis, growth and their distribution. Marine Environ Res 184:105877. https://doi.org/10.1016/j.marenvres.2023.105877

Kim S-K (ed)(2015) Handbook of marine microalgae. Academic Press, London

Masclaux-Daubresse C, d'Andrea S, Bouchez I, Cacas J-L (2020) Reserve lipids and plant autophagy. Journal of Experimental Botany 71:2854-2861. https://doi.org/10.1093/jxb/eraa082

Mišić Radić T, Čačković A, Penezić A, Dautović J, Lončar J, Omanović D, Juraić K, Ljubešić Z (2021) Physiological and morphological response of marine diatom *Cylindrotheca closterium* (Bacillariophyceae) exposed to cadmium. Eur J Phycol 56:24-36. https://doi.org/10.1080/09670262.2020.1758347

Mišić Radić T, Vukosav P, Komazec B, Formosa-Dague C, Domazet Jurašin D, Peharec Štefanić P, Čačković A, Juraić K, Ivošević DeNardis N (2022) Nanoplastic-Induced Nanostructural, Nanomechanical, and Antioxidant Response of Marine Diatom *Cylindrotheca closterium*. Water 14:2163. https://doi.org/10.3390/w14142163

Monteiro I, Schüler LM, Santos E, et al (2023) Two-stage lipid induction in the microalga Tetraselmis striata CTP4 upon exposure to different abiotic stresses. Renewable Energy 208:693–701. https://doi.org/10.1016/j.renene.2023.03.103

Murphy GEP, Romanuk TN, Worm B (2020) Cascading effects of climate change on plankton community structure. Ecol Evol 10:2170-2181. https://doi.org/10.1002/ece3.6055

Niemelä PS, Hyvönen MT, Vattulainen I (2006) Influence of chain length and unsaturation on sphingomyelin bilayers. Biophys J 90:851-63. https://doi.org/10.1529/biophysj.105.067371

Novak T, Godrijan J, Marić Pfannkuchen D, Djakovac T, Medić N, Ivančić I, Mlakar M, Gašparović B (2019) Global warming and oligotrophication lead to increased lipid production in marine phytoplankton. Sci Total Environ 668:171-183. https://doi.org/10.1016/j.scitotenv.2019.02.372

Novosel N, Kasum D, Žutinić P, Legović T, Ivošević DeNardis N (2020) Short-term effect of cadmium on the motility of three flagellated algal species. J Appl Phycol 32:4057-4067. https://doi.org/10.1007/s10811-020-02283-1

Novosel N, Mišić Radić T, Zemla J, Lekka M, Čačković A, Kasum D, Legović T, Žutinić P, Gligora Udovič M, Ivošević DeNardis N (2022a) Temperature-induced response in algal cell surface properties and behaviour: an experimental approach. J Appl Phycol 34:243-259. https://doi.org/10.1007/s10811-021-02591-0

Novosel N, Mišić Radić T, Levak Zorinc M, Zemla J, Lekka M, Vrana I, Gašparović B, Horvat L, Kasum D, Legović T, Žutinić P, Gligora Udovič M, Ivošević DeNardis N (2022b) Salinity induced chemical, mechanical and behavioral changes in marine microalgae. J Appl Phycol 34:1293–1309. https://doi.org/10.1007/s10811-022-02734-x

Pick U, Avidan O (2017) Triacylglycerol is produced from starch and polar lipids in the green alga Dunaliella tertiolecta. Journal of Experimental Botany 68:4939-4950. https://doi.org/10.1093/jxb/erx280

Pillet F, Dague E, Pečar Ilić J, Ružić I, Rols M-P, Ivošević DeNardis N (2019) Changes in nanomechanical properties and adhesion dynamics of algal cells during their growth. Bioelectrochemistry 128:154-162. https://doi.org/10.1016/j.bioelechem.2019.02.011

Pletikapić G, Berquand A, Mišić Radić T, Svetličić V (2012) Quantitative nanomechanical mapping of marine diatom in seawater using peak force tapping atomic force microscopy. J Phycol 48:174-185. https://doi.org/10.1111/j.1529-8817.2011.01093.x

Pletikapić G, Ivošević DeNardis N (2017) Application of surface analytical methods for hazardous situation in the Adriatic Sea: Monitoring of organic matter dynamics and oil pollution. Nat Hazards Earth Syst Sci 17:31-44. https://doi.org/10.5194/nhess-17-31-2017

RStudio Team (2023). RStudio: Integrated Development Environment for R. Posit Software, PBC, Boston, MA. http://www.posit.co/.

R Core Team (2022) R: A language and environment for statistical computing. R Foundation for Statistical Computing, Vienna, Austria. https://www.R-project.org/.

Royston P (1995) Remark AS R94: A remark on Algorithm AS 181: The WW test for normality. Applied Statistics 44:547.551. https://doi.org/10.2307/2986146

Sader JE, Larson I, Mulvaney P, White LR (1995) Method for the calibration of atomic force microscope cantilevers. Rev Sci Instrum 66:3789–3798. https://doi.org/10.1063/1.1145439

Schriber CL, Venable ME (2019) The Effects of Environmental Stressors on Aggregation in *Parachlorella kessleri*. Journal of Environmental Protection 10:1657-1676. https://doi.org/10.4236/jep.2019.1012099

Siegenthaler P-A (1998) Molecular organization of acyl lipids in photosynthetic membranes of higher plants. In: Siegenthaler P A, Murata N (eds) Lipids in photosynthesis. Kluwer Academic Publishers, Dordrecht, The Netherlands, pp 119–144. https://doi.org/10.1007/0-306-48087-5_7

Sneddon IN (1965) The relation between load and penetration in the axisymmetric boussinesq problem for a punch of arbitrary profile. Int J Eng Sci 3:47-57. https://doi:10.1016/0020-7225(65)90019-4

Srirangan S, Sauer ML, Howard B, Dvora M, Dums J, Backman P, Sederoff H (2015) Interaction of Temperature and Photoperiod Increases Growth and Oil Content in the Marine Microalgae *Dunaliella viridis*. PLoS ONE 10: e0127562. https://doi.org/10.1371/journal.pone.0127562

Svetličić V, Balnois E, Žutić V, Chevalet J, Hozić Zimmermann A, Kovač S, Vdović N (2006) Electrochemical detection of gel microparticles in seawater. Croat Chem Acta 79:107-113. https://hrcak.srce.hr/2619

Thompson GA (1996) Lipids and membrane function in green algae. Biochim Biophys Acta - Lipids Lipid Metab 1302:17-45. https://doi.org/10.1016/0005-2760(96)00045-8

Van de Waal DB, Litchman E (2020) Multiple global change stressor effects on phytoplankton nutrient acquisition in a future ocean. Philos Trans R Soc Lond B Biol Sci 375:20190706. https://doi.org/10.1098/rstb.2019.0706

Velasco J, Gutiérrez-Cánovas C, Botella-Cruz M, Sánchez-Fernández D, Arribas P, Carbonell JA, Millán A, Pallarés S (2019) Effects of salinity changes on aquatic organisms in a multiple stressor context. Philos Trans R Soc Lond B Biol Sci 374:20180011. https://doi.org/10.1098/rstb.2018.0011

Vrana I, Alempijevic SB, Novosel N, Ivošević DeNardis N, Zigon D, Ogrinc N, Gašparović B (2022) Hyposalinity induces significant polar lipid remodeling in the marine microalga *Dunaliella tertiolecta* (Chlorophyceae). J Appl Phycol 34:1457-1270. https://doi.org/10.1007/s10811-022-02745-8

Vrana I, Gašparović B, Geček S, Godrijan J, Novak T, Kazazić SP, Mlakar M, Kužat N, Pfannkuchen M, Marić Pfannkuchen D (2023) Successful acclimation of marine diatoms *Chaetoceros curvisetus/pseudocurvisetus* to climate change. Limnol Oceanogr. https://doi.org/10.1002/lno.12293

Wu X, Liu H, Ru Z, Tu G, Xing L, Ding Y (2021) Meta-analysis of the response of marine phytoplankton to nutrient addition and seawater warming. Marine Environ Res 168:105294. https://doi.org/10.1016/j.marenvres.2021.105294

Zelazny AM, Shaish A, Pick U (1995) Plasma-membrane sterols are essential for sensing osmotic changes in the halotolerant alga *Dunaliella*. Plant physiol 109:1395-1403. https://doi.org/10.1104/pp.109.4.1395

Zhang X, Tan L, Cai Q, Ye L (2022) Environmental factors indirectly reduce phytoplankton community stability via functional diversity. Front Ecol Evol 10:990835. https://doi.org/10.3389/fevo.2022.990835

Žutić V, Svetličić V, Ivošević N, Hozić A, Pečar O (2004) Northern Adriatic mesocosm experiment Rovinj 2003: dynamics of organic microparticles studied by the electrochemical technique. Period Biol 106:67-74

Fig. 1 Microcosm experimental setup in an outdoor swiming pool at the
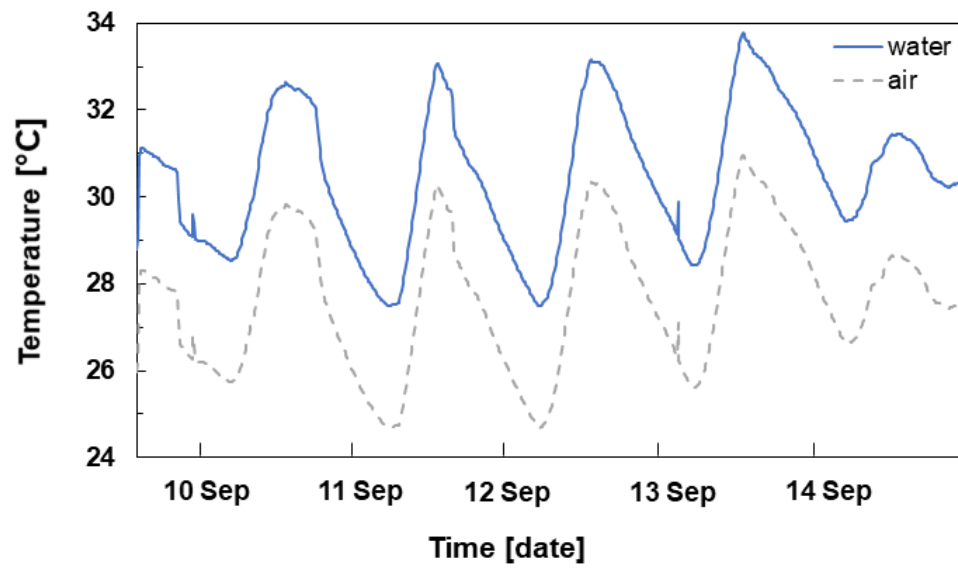Ruđer Bošković Institute, Zagreb, Croatia

Fig. 2 Variation of water and air temperatures in the swimming pool during the microcosm experiment conducted in September 2022
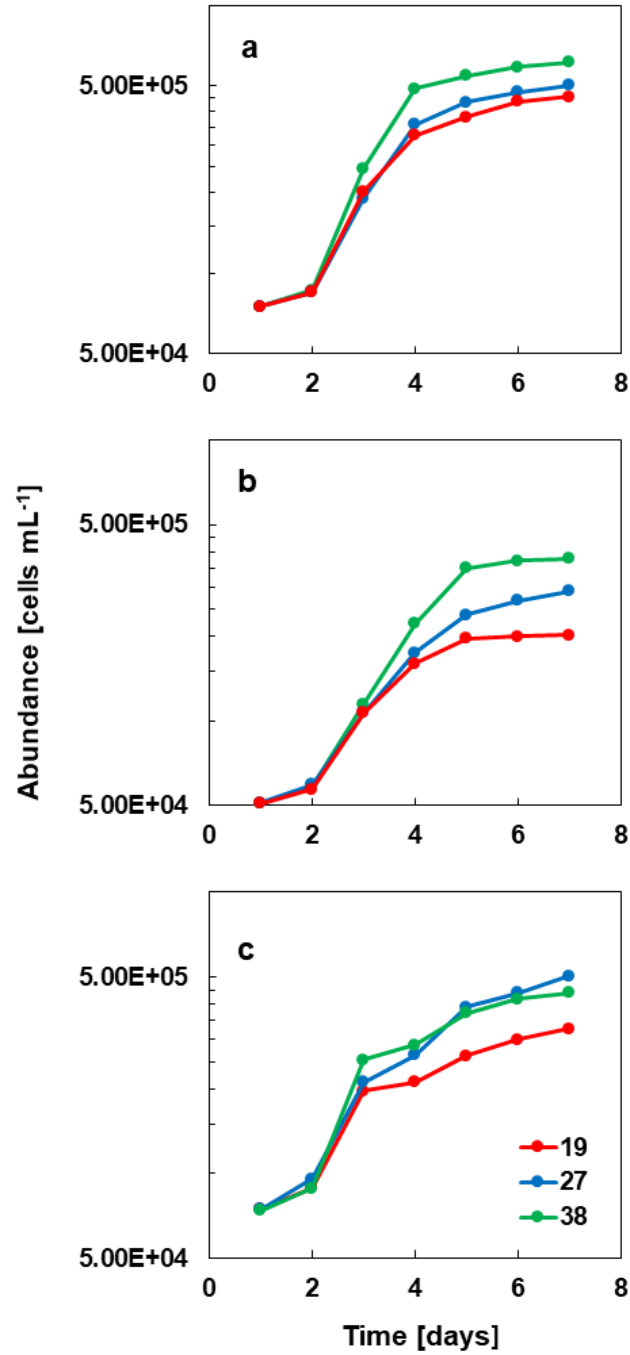
Fig. 3 Growth curves of DT, TS, and CC under environmental stressors (salinities of 19, 27, 38, and elevated temperatures) in near-natural conditions
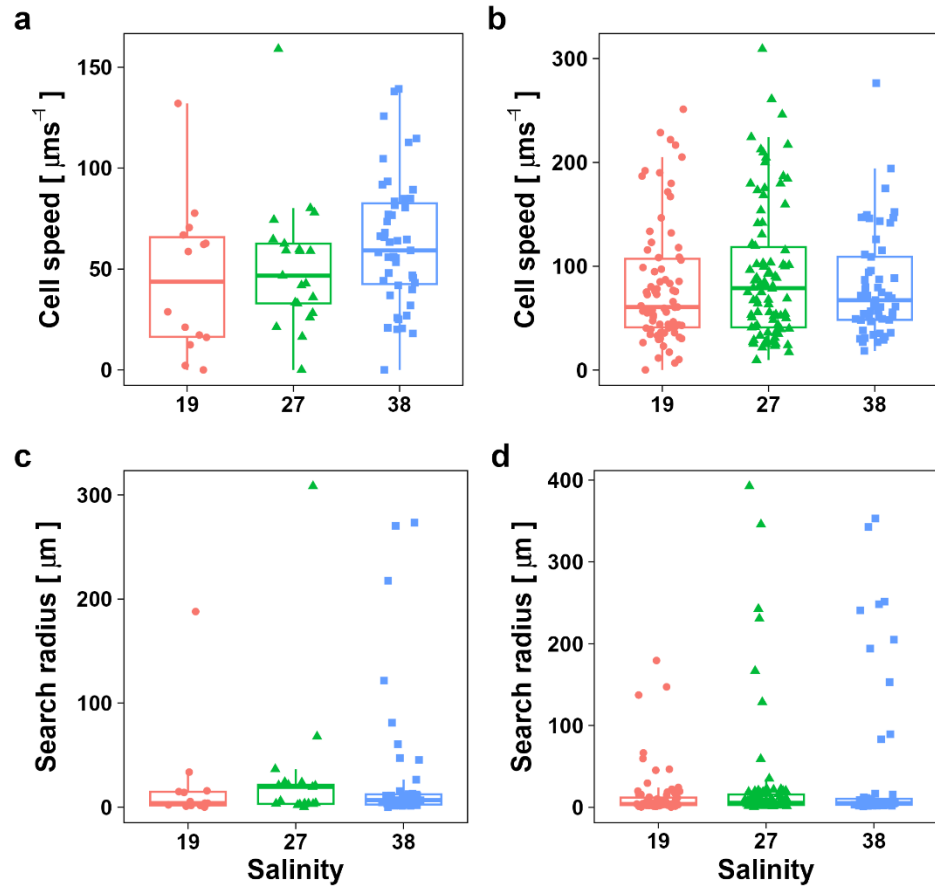
Fig. 4 Box plots for cell speed and search radius for the species DT (a, c) and TS (b, d) under environmental stressors in near-natural conditions
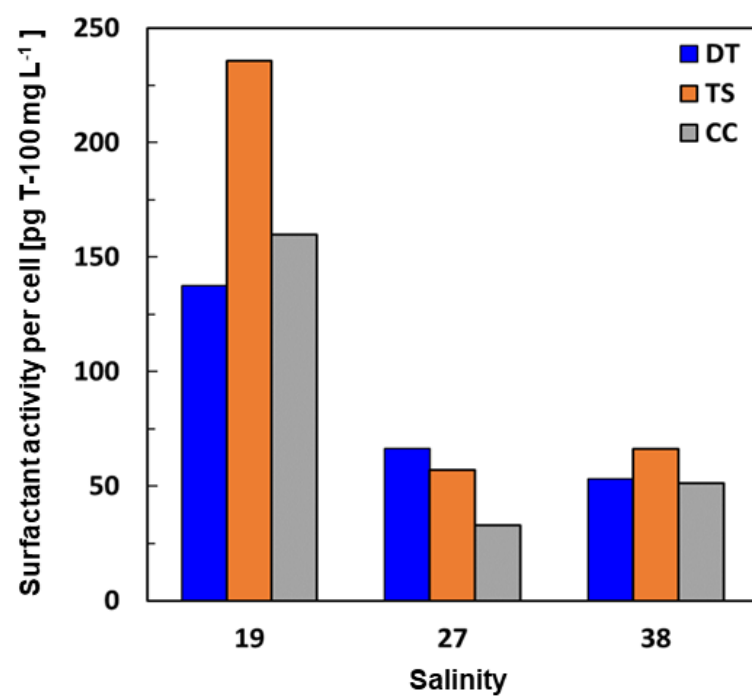
Fig. 5 Surfactant activity of studied algal species under environmental stressors in near-natural conditions
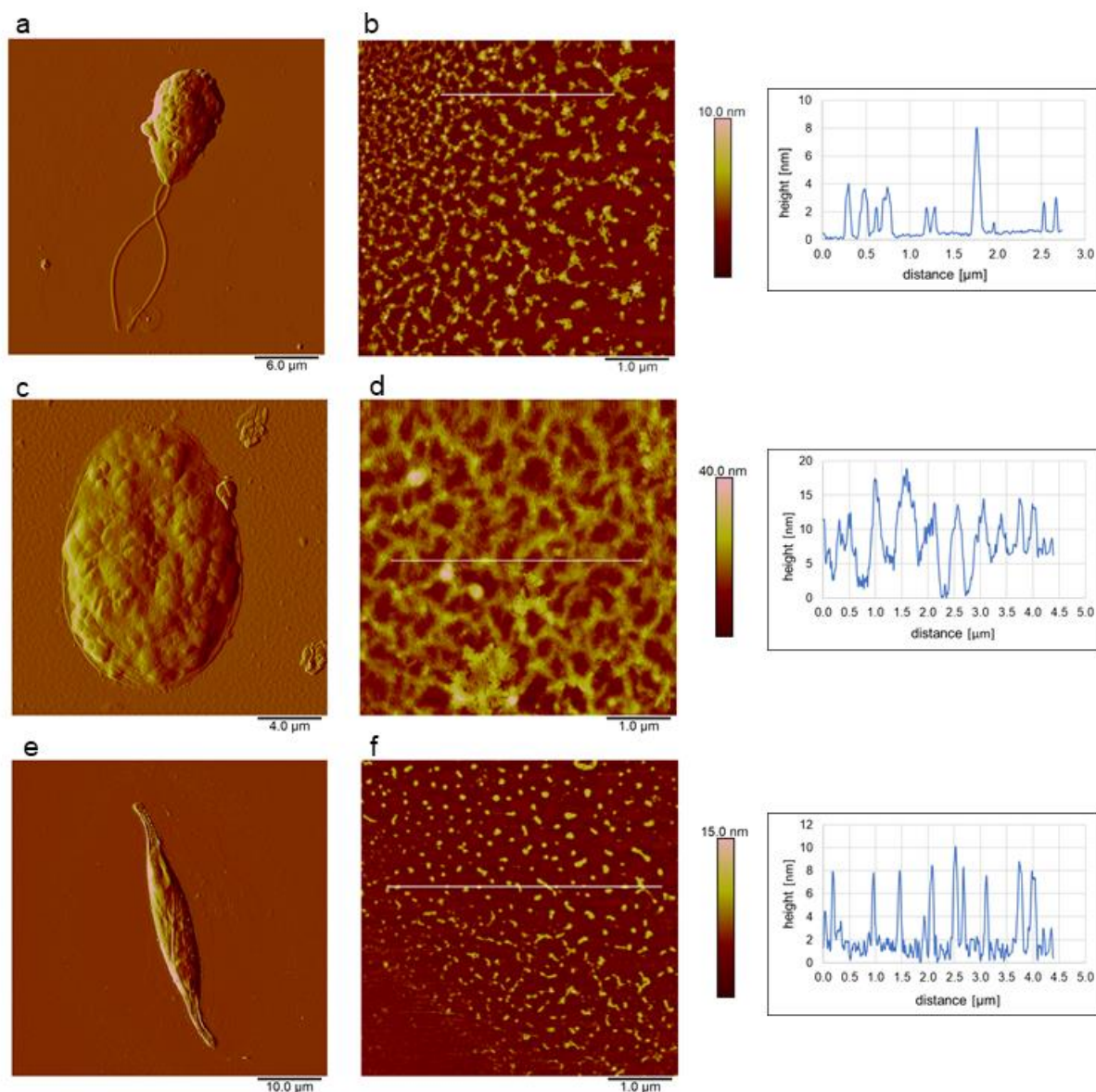
Fig. 6 AFM images of the cells and extracellular polymers of DT, TS, and CC grown at selected salinities. Cell of DT grown at a salinity of 19 (a); EPS material around the DT cell with vertical profile along the indicated line (b); TS cell grown at a salinity of 38 (c); EPS network around the TS cell with vertical profile along the indicated line (d); cell of CC grown at a salinity of 27 (e); EPS material around CC with vertical profile along the indicated line (f). Images were acquired in contact mode in air and presented as defection data (a, c, e) and height data with vertical profiles along the indicated lines (b, d, f). Scan sizes: 30 µm × 30 µm (a); 5 µm × 5 µm, vertical scale 100 nm (b); 20 µm × 20 µm (c); 5 µm × 5 µm, vertical scale 40 nm (d); 50 µm × 50 µm (e); 5 µm × 5 µm, vertical scale 15 nm (f)
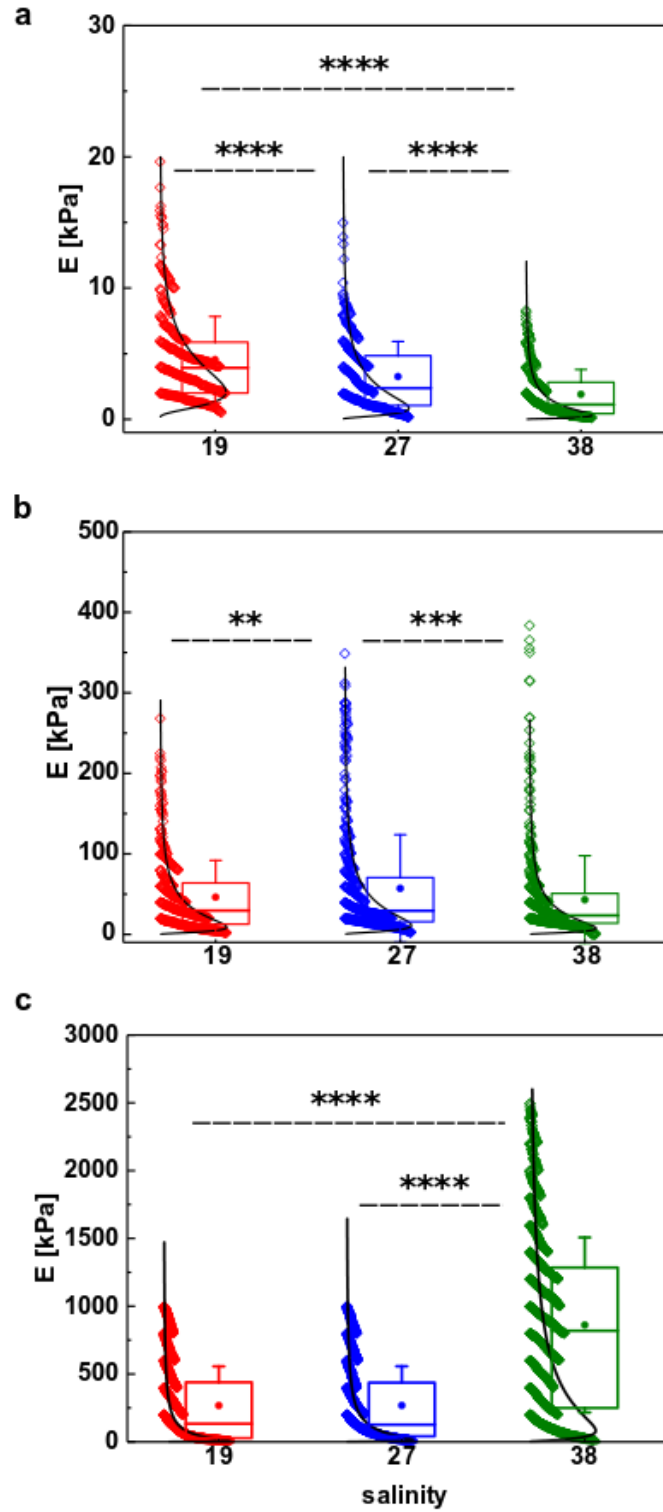
Fig. 7 Box plots depicting Young's modulus distributions for DT (a), TS (b), and CC (c) cells under environmental stressors in near-natural conditions. A whiskered box reflects the median interquartile range (Q3-Q1). The Kruskal-Wallis ANOVA test yielded statistical significance at the level of 0.05 (**** p<0.0001,*** p< 0.001, ** p<0.01, *p<0.05)
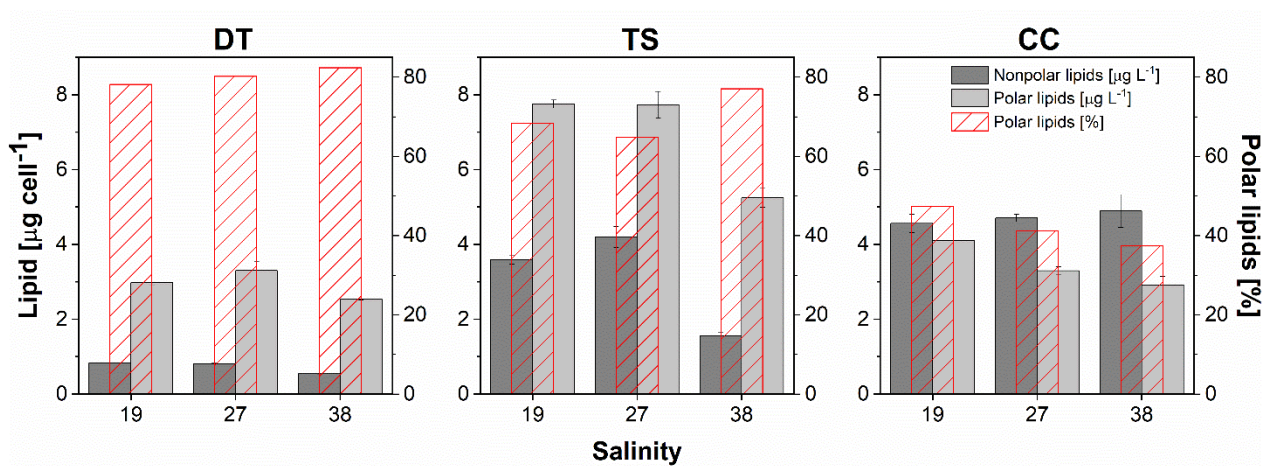
Fig. 8 Nonpolar and polar lipid content (solid columns) and the contribution of polar lipids to total cell lipids (pattern columns) of DT, TS, and CC under environmental stressor in near-natural conditions. Data are shown as mean ± SD
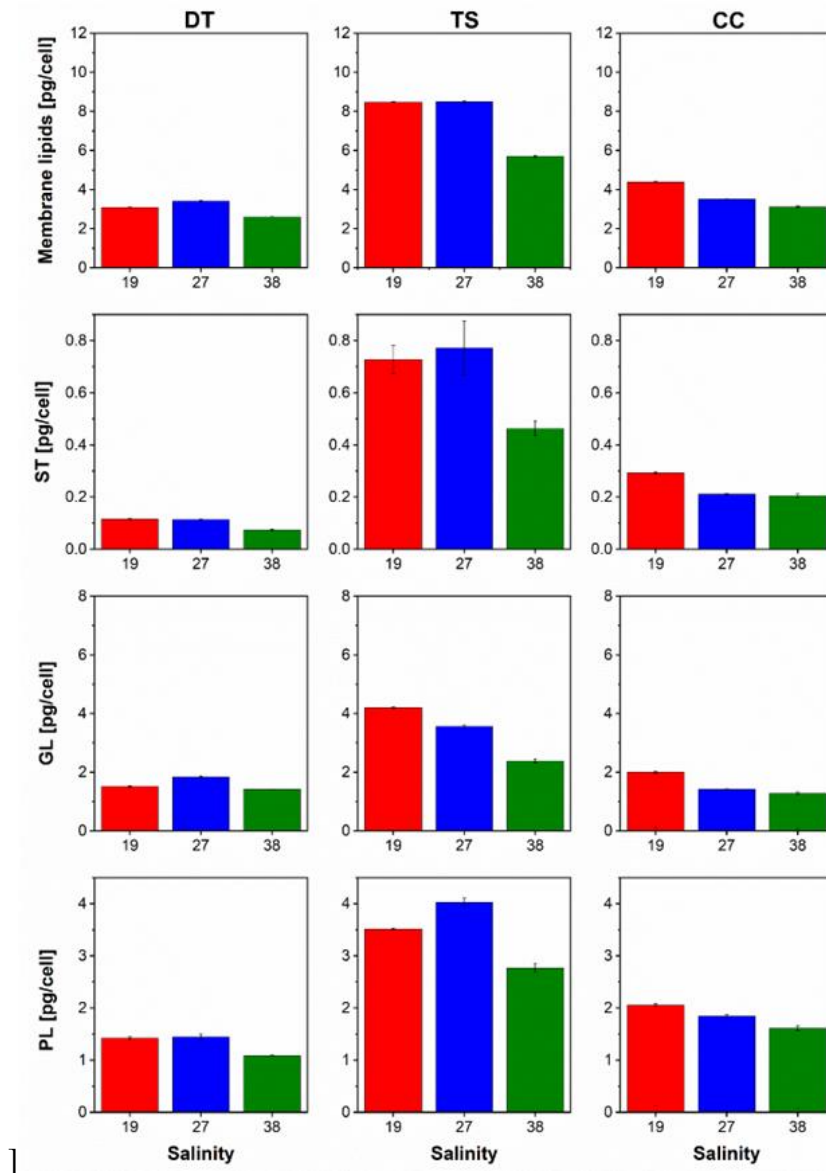
Fig. 9 Membrane lipid content of DT, TS, and CC
under environmental stressors in near-natural conditions. Data are shown as mean ± SD

Table 1 Hydrophobic properties of algal cells under environmental stressors in near-natural conditions. Hydrophilic properties are indicated by (+) and hydrophobic behavior by (-). The value zero means a balance between hydrophobic and hydrophilic moeities on the cell surface.

S	DT	TS	CC
19	+	0	+
27	+	0	+
38	+	-	+

Supplementary material

Behavior and surface properties of microalgae indicate environmental changes

Journal of Applied Phycology

N. Ivošević DeNardis[1*], N. Novosel Vlašić [1], T. Mišić Radić[1], J. Zemła[2], M. Lekka[2], I. Demir-Yilmaz[3,4], C. Formosa Dague[3], M. Levak Zorinc[1], I. Vrana[1], K. Juraić[1], L. Horvat[1], P. Žutinić[5], M. Gligora Udovič[5], B. Gašparović[1]

[1]Ruđer Bošković Institute, Zagreb, Croatia, [2]Institute of Nuclear Physics Polish Academy of Sciences, Kraków, Poland, [3] TBI, Université de Toulouse, INSA, INRAE, CNRS, Toulouse, France, [4]LAAS, Université de Toulouse, CNRS, Toulouse, France, [5]Department of Biology, Faculty of Science, University of Zagreb, Zagreb, Croatia

Corresponding author:
N. Ivošević DeNardis
Tel: +385 1 4561-128
E-mail address: ivosevic@irb.hr

DT, salinity 19 **DT, salinity 27** **DT salinity 38**

TS, salinity 19 **TS, salinity 27** **TS, salinity 38**

CC, salinity 19 **CC, salinity 27** **CC, salinity 38**
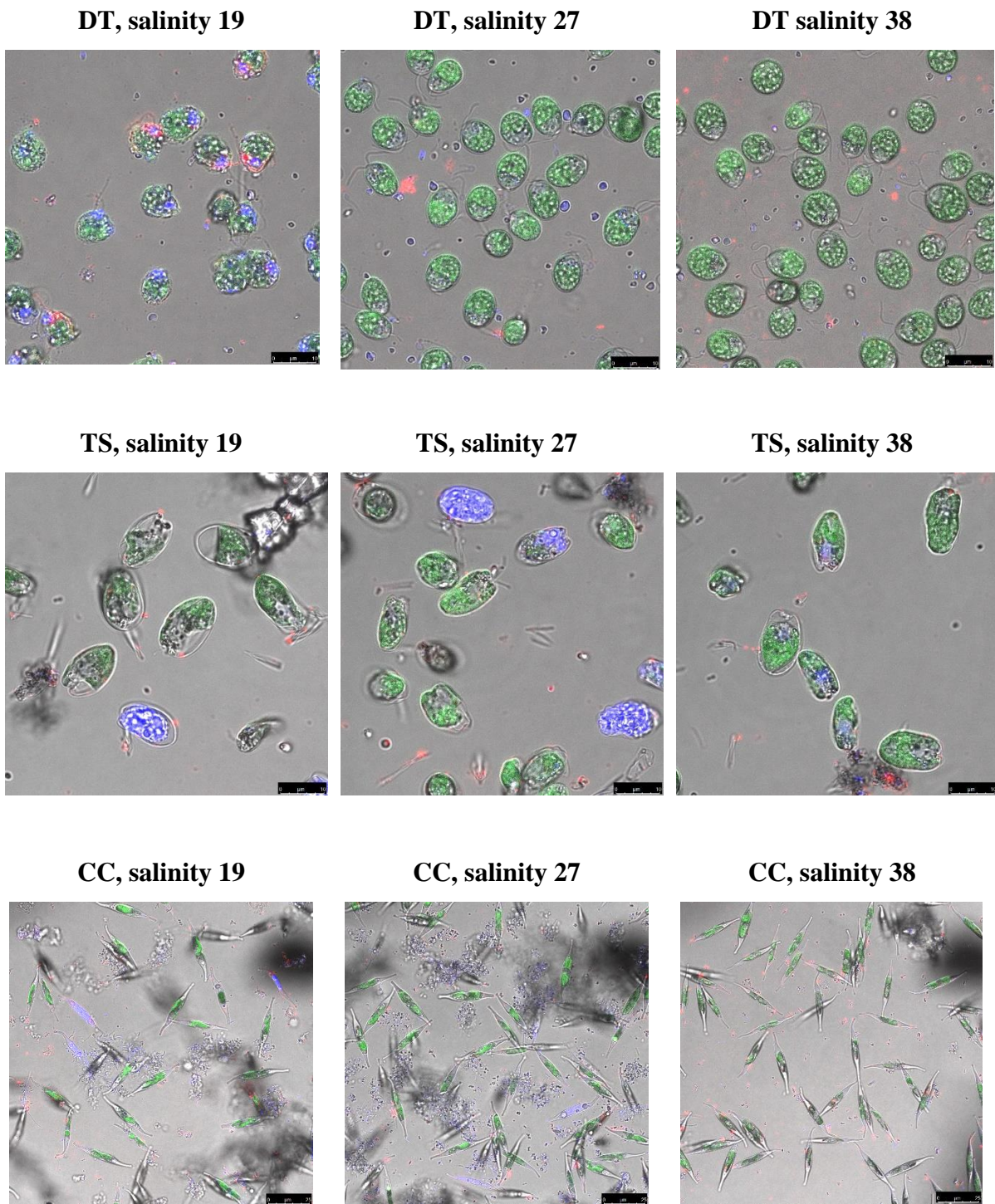
Fig. S1 Confocal images of DT, TS and CC grown under environmental stressors in near-natural conditions. For DT, and TS bar denotes 10 μm, while for CC bar denotes 25 μm

Salinity 19   **Salinity 27**   **Salinity 38**
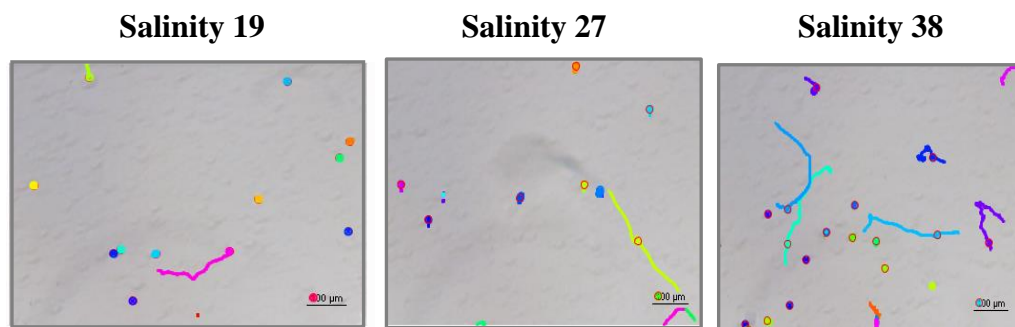
Fig. S2 Reconstructed trajectories of DT cells grown under environmental stressors in near-natural conditions. The colored circles represent cells, and lines show their trajectories

Salinity 19 **Salinity 27** **Salinity 38**
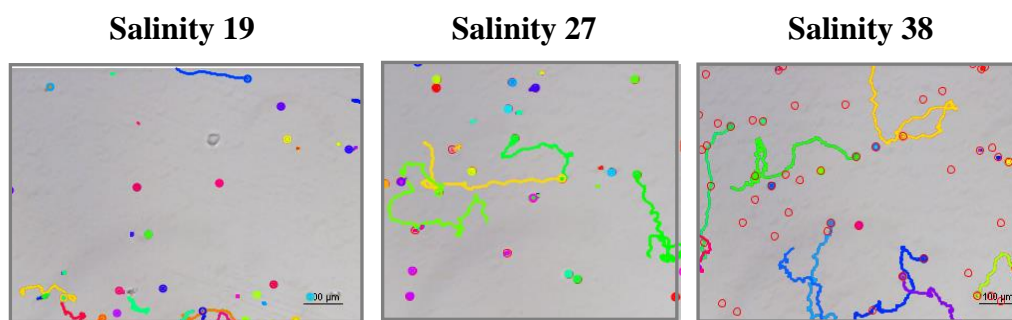
Fig. S3 Reconstructed trajectories of TS cells grown under environmental stressors in near-natural conditions. The colored circles represent cells, and lines show their trajectories
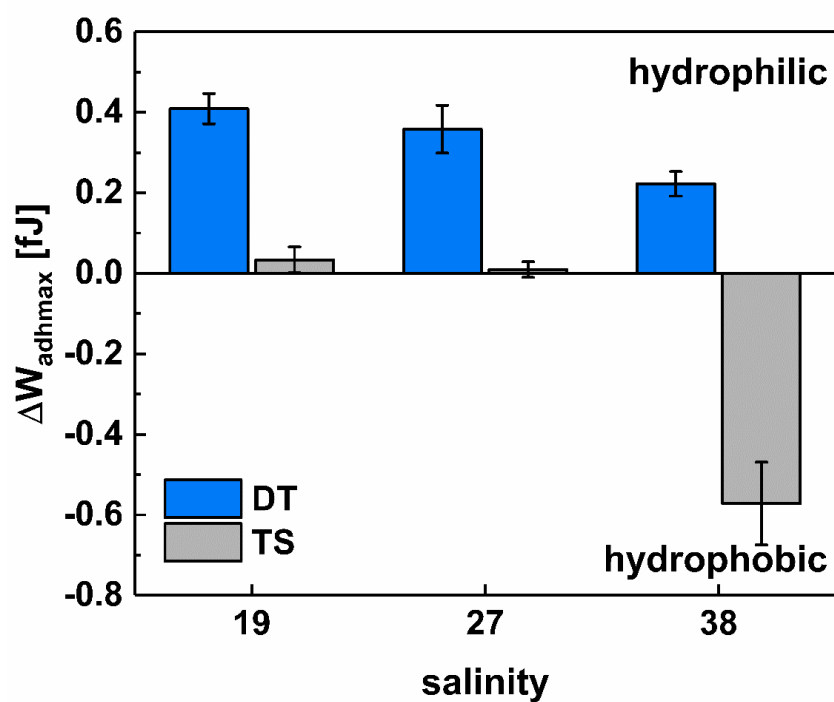
Fig. S4 The ratio of hydrophilic and hydrophobic properties of a DT and TS cell surface under environmental stressors in near-natural conditions.

Data are shown as maximum $\Delta W_{adh} \pm$ maximum error

Table S1 Growth rate (μ) and doubling time (T) of microalgal species in the exponential growth phase under environmental stressors in near-natural conditions.

S	DT		TS		CC	
	μ [d^{-1}]	T [d]	μ [d^{-1}]	T [d]	μ [d^{-1}]	T [d]
19	0.32	2.16	0.31	2.27	0.14	4.81
27	0.41	1.67	0.40	1.72	0.31	2.26
38	0.40	1.75	0.56	1.25	0.19	3.63

Table S2.1 Selected salinities, sample size, number of vibrating cells with corresponding average speed and average search radius and number of moving cells with corresponding average speed, standard error of the mean speed, average search radius, and standard error of the mean search radius for DT.

S	Sample size	No. vibrating	Avg. speed [μms^{-1}]	Avg. search radius [μm]	No. Moving	Avg. speed [$\mu m\ s^{-1}$]	SEM speed [$\mu m\ s^{-1}$]	Avg. search radius [μm]	SEM search radius [μm]
19	14	6	14	1	8	68	11	35	22
27	21	4	27	2	17	57	7	36	17
38	47	13	30	2	34	76	5	39	12

Table S2.2 Selected salinities, sample size, cells speed [µm s^{-1}] (a) and search path [µm] (b) data of DT obtained by the analysis of 82 individual cells. Q1 – the first quartile; Q3 – the third quartile, SD – standard deviation, SEM – standard error of the mean.

(a) Speed

S	Size	Min	Q1	Median	Mean	Q3	Max	SD	SEM
19	14	0	16	44	45	66	132	37	10
27	21	0	33	47	51	63	159	33	7
38	47	0	43	59	63	83	139	32	5

(b) Search radius

S	Size	Min	Q1	Median	Mean	Q3	Max	SD	SEM
19	14	0	2	4	21	15	188	49	13
27	21	0	3	19	29	21	308	66	14
38	47	0	2	7	29	12	273	64	9

Table S3.1 Selected salinities, sample size, number of vibrating cells with corresponding average speed and average search radius and number of moving cells with corresponding average speed, standard error of the mean speed, average search radius, and standard error of the mean search radius for TS.

S	Sample size	No. vibrating	Avg. speed [μms^{-1}]	Avg. search radius [μm]	No. Moving	Avg. speed [μm s^{-1}]	SEM speed [μm s^{-1}]	Avg. search radius [μm]	SEM search radius [μm]
19	75	25	47	2	50	99	8	22	5
27	90	24	32	2	66	114	7	33	3
38	57	13	41	2	44	93	7	54	14

Table S3.2 Selected salinities, sample size, cells speed [μm s^{-1}] (a) and search path [μm] (b) data of TS obtained by the analysis of 222 individual cells. Q1 – the first quartile; Q3 – the third quartile, SD – standard deviation, SEM – standard error of the mean.

(a) Speed

S	Size	Min	Q1	Median	Mean	Q3	Max	SD	SEM
19	75	0	41	61	82	107	251	59	7
27	90	9	41	79	92	118	309	65	7
38	57	18	48	67	81	109	276	50	7

(b) Search radius

S	Size	Min	Q1	Median	Mean	Q3	Max	SD	SEM
19	75	0	3	4	14	12	179	31	4
27	90	0	3	5	24	15	392	66	7
38	57	1	3	5	42	10	353	89	13

Table S3.3 Results of Shapiro-Wilk normality test for cell speed [μm s^{-1}] (a) and search radius [μm] data presented in Fig. 4 and Tables 2.2 and 3.2.

	Salinity	Cell speed		Search radius	
		W	p	W	p
DT	19	0.902	0.121	0.390	9.10e-07
	27	0.866	0.00830	0.388	2.20e-08
	38	0.973	0.354	0.442	3.95e-12
TS	19	0.879	3.26e-06	0.413	9.02e-16
	27	0.889	1.32e-06	0.335	2.78e-18
	38	0.870	1.89e-05	0.489	8.54e-13

Table S3.4 Results of Kruskal-Wallis ANOVA test (p-values) for cell speed [μm s^{-1}] (a) and search radius [μm] data presented in Fig. 4 and Tables 2.2 and 3.2.

	Cell speed			Search radius		
	Salinity	19	27	Salinity	19	27
DT	27	0.315	-	27	0.710	-
	38	0.626	0.017	38	0.910	0.770
	Salinity	19	27	Salinity	19	27
TS	27	0.146	-	27	0.590	-
	38	0.979	0.059	38	1.000	0.430

Table S4 Cell dimensions (l – length, w – width, h – height) and surface roughness (R_a) *of* DT, TS and CC cells grown under environmental stressors in near-natural conditions based on analysis of AFM images.

Salinity	DT				TS				CC			
	l [µm]	w [µm]	h [µm]	R_a [nm]*	l [µm]	w [µm]	h [µm]	R_a [nm] **	l [µm]	w [µm]	h [µm]	R_a [nm]*
19	11.3±1.1	6.54±0.74	2.16±0.75	12.7±2.7	14.9±0.9	11.90±0.88	1.49±0.34	32.0±10.0	39.1±1.7	5.80±0.61	0.76±0.20	3.9±1.1(v) 4.9±0.9 (g)
27	10.35±0.98	5.85±0.86	2.81±0.36	12.4±1.6	15.2±0.9	11.9±1.3	1.76±0.43	35.5±6.5	39.7±1.6	5.35±0.49	0.57±0.05	3.7±0.9(v) 3.9±0.7 (g)
38	10.4±1.0	6.27±0.86	2.89±0.52	16.1±4.2	16.6±2.0	11.3±1.0	1.98±0.49	36.4±6.0	39.8±1.6	5.50±0.77	0.67±0.21	3.1±0.7(v) 3.2±0.8 (g)

v – valve; g – girdle bands, * roughness analysis performed on area 500 x 500 nm, **roughness analysis performed on area 2 x 2 µm